

One-pot synthesis of Fe₃O₄/C nanocomposites by PEG-assisted co-precipitation as anode materials for high-rate lithium-ion batteries

Yanchun Ma · Yudai Huang · Xingchao Wang ·
Dianzeng Jia · Xincun Tang

Received: 26 April 2014 / Accepted: 14 August 2014 / Published online: 3 September 2014
© Springer Science+Business Media Dordrecht 2014

Abstract Fe₃O₄/C nanocomposites have been prepared by one-pot PEG-assisted co-precipitation method. The structure and morphology of the as-prepared materials were analyzed by X-ray diffraction and transmission electron microscopy. The results showed that Fe₃O₄/C nanocomposites were well crystallized. Carbon nanoparticles dispersed among Fe₃O₄ particles forming a carbon layer, which prevent Fe₃O₄ particles from contacting each other. Electrochemical performance tests showed that Fe₃O₄/C nanocomposites keep at a high discharge capacity of 902.4 mAh g⁻¹ at 1 C after 110 cycles. Furthermore, the samples showed much improved rate capability and better cycle stability compared with pure Fe₃O₄. The excellent electrochemical performance of Fe₃O₄/C nanocomposites can be attributed to unique nanostructure and existence of amorphous carbon in the composites. The existence of the amorphous carbon not only enhanced electric conductivity, but also buffered volume variation of Fe₃O₄/C nanocomposites during charge/discharge process.

Keywords One-pot · Fe₃O₄/C nanocomposites · Co-precipitation · Lithium-ion battery · Anode material · Energy storage

Introduction

With the daily depletion of petroleum resources, energy storage has become a crucial issue. Lithium-ion batteries (LIBs), as novel energy storage device, were extensively studied during past years. The properties of anode materials play a significant role in performance of LIBs (Bruce et al. 2008). Fe₃O₄ is an attractive candidate for anode material of LIBs due to its environment friendliness, high abundance and high theoretical capacities (924 mAh g⁻¹) (Duan et al. 2012). Nevertheless, a large specific volume variation usually occurs in the host matrices of the metal oxide during charge/discharge process, and Fe nanocrystals come from lithiation process can catalyze decomposition the outer solid electrolyte interphase (SEI) (He et al. 2013), which will lead to rapid capacity decay and high-initial irreversible capacity loss. In previous research, two main kinds of strategies have been considered to improve the electrochemical performance of Fe₃O₄. Controlling Fe₃O₄ nanostructures is one way to partially accommodate the volume variation during Li⁺ insert/extract process and reduce diffusion path for Li⁺, which can improve their rate capability and capacity retention. Nanostructures,

Y. Ma · Y. Huang (✉) · X. Wang · D. Jia (✉) · X. Tang
Key Laboratory of Material and Technology for Clean Energy, Ministry of Education, Key Laboratory of Advanced Functional Materials, Autonomous Region, Institute of Applied Chemistry, Xinjiang University, Ürümqi, 830046, Xinjiang, China
e-mail: huangyd@xju.edu.cn

D. Jia
e-mail: jdz@xju.edu.cn

such as hollow particles (Chen et al. 2012b), porous nanoparticles (Chen et al. 2012a), nanorods (Chen et al. 2011b), nanotubes (Gao et al. 2011) etc., have been fabricated. Another strategy is to enhance electronic conductivity through synthesis of Fe_3O_4 nanocomposites. Many materials with high electronic conductivities, such as RuO_2 (Liu et al. 2012), SnO_2 (Wu et al. 2011), and carbon (C) (Zhang et al. 2008), have been selected to construct the conducting networks, among them, C is an appealing choice. C is a very stable anode material in LIBs due to small volume change during Li^+ insert/extract process. It acts as a better cushioning layer to effectively buffer volume variation of the inner active materials during charge/discharge process. Furthermore, C layer has a vital role in enhancing electronic conductivity of electrode materials (Zhou et al. 2014).

However, there is less work focuses on combine controlling nanostructures with connecting C to improve the electrochemical properties of Fe_3O_4 . And for preparation of $\text{Fe}_3\text{O}_4/\text{C}$ nanocomposites, most methods involve many complicated steps, such as centrifugation or suction filtration for product collection, rinsing with water and ethanol, and oven drying (Zhong et al. 2011). It is therefore desirable to develop a high-yield and simple synthesis method to facilitate the applications of such material.

Here, $\text{Fe}_3\text{O}_4/\text{C}$ nanocomposites were prepared by one-pot PEG-assisted co-precipitation method with simple steps by combine controlling nanostructures with connecting C. The precursors of $\text{Fe}_3\text{O}_4/\text{C}$ nanocomposites were synthesized by heating the mixture of $\text{Fe}(\text{NO}_3)_3 \cdot 9\text{H}_2\text{O}$, PEG 400 (PEG: polyethylene glycol; 400: polymerization degree) and $\text{H}_2\text{C}_2\text{O}_4 \cdot 2\text{H}_2\text{O}$ in thermostatic water bath. In the reaction process, excess $\text{H}_2\text{C}_2\text{O}_4 \cdot 2\text{H}_2\text{O}$ acted as complexing agent with $\text{Fe}(\text{NO}_3)_3 \cdot 9\text{H}_2\text{O}$ and formed soluble complex ($[\text{Fe}(\text{C}_2\text{O}_4)_3]^{3-}$), the PEG 400 chains surrounding the ($[\text{Fe}(\text{C}_2\text{O}_4)_3]^{3-}$) complex helped the complex dispersed in the solution and acted as C source afterward (Gong et al. 2014). After precipitation and calcination, $\text{Fe}_3\text{O}_4/\text{C}$ nanocomposites were prepared. Herein, C nanoparticles have important role in improving electrochemical performance of $\text{Fe}_3\text{O}_4/\text{C}$ nanocomposites, which enhance electric conductivity and buffer volume variation of the nanocomposites during charge/discharge process. Thus the as-synthesized $\text{Fe}_3\text{O}_4/\text{C}$ nanocomposites exhibit excellent electrochemical performance, with ultra-high rate capabilities, which

is much improved relative to that of pure Fe_3O_4 . Compared with other Fe-based materials (Lang and Xu 2013; Zhao et al. 2012a), $\text{Fe}_3\text{O}_4/\text{C}$ nanocomposites obtained in this work show better cycling performance.

Experimental section

Experimental

$\text{Fe}_3\text{O}_4/\text{C}$ nanoparticles were prepared by one-pot PEG-assisted co-precipitation method with simple steps. All reagents are analytically pure and used without further purification. In a typical experiment, 2.52 g $\text{H}_2\text{C}_2\text{O}_4 \cdot 2\text{H}_2\text{O}$ and 2.00 g PEG 400 were dissolved in 100 mL deionized water, followed by addition of 2.02 g $\text{Fe}(\text{NO}_3)_3 \cdot 9\text{H}_2\text{O}$ under magnetic stirring for 5 h to form a homogenous mixture solution. The mixture was transferred to a thermostat water bath and then maintained at 80 °C for 72 h and allowed to cool down to room temperature naturally. The faint yellow precipitate was prepared. After calcining the precipitate under argon atmosphere at 600 °C for 6 h, the $\text{Fe}_3\text{O}_4/\text{C}$ nanoparticles were obtained. For comparison, pure Fe_3O_4 particles were prepared by the same procedure without addition of PEG 400.

Characterization of synthesized material

The crystal structures of the samples were investigated by X-ray diffraction (XRD, Bruker D8 Advance) with $\text{Cu K}\alpha$ radiation. Raman measurement was employed to verify the chemical bonding characteristics of carbon with Raman microscope (Bruker Senterra R200-L) using a laser line of 532 nm as the excitation source. To understand the approximate content of carbon in the synthesized product, thermal gravimetric analysis (Netzsch Sta 449 F3) of the samples were employed from room temperature to 850 °C under air ventilation at a heating rate of 10 °C min^{-1} . The morphological characteristics of the products were investigated by transmission electron microscopy (TEM, H-600, Hitachi, Japan). The working electrodes were prepared by mixing the active materials, acetylene black, and polyvinylidene fluoride at a weight ratio of 75:15:10 in *N*-methyl pyrrolidinone solvent. The mixtures were pasted on pure Cu foil, and

then dried at 110 °C in a vacuum oven for 12 h for use in coin-type cells (2032), which were assembled in an argon-filled glove box. A Celgard 2300 microporous polyethylene membrane was used as the separator. The electrolyte was 1 M LiPF₆ in a 1:1 (volume ratio) mixture of ethylene carbonate and dimethyl carbonate, and a lithium foil was as the counter electrode. The charge/discharge measurements were carried out on a battery test system (CT2001A, Land, China) in the voltage range between 0.0 and 3.0 V at room temperature. The specific capacities were calculated based on the total mass of active materials including Fe₃O₄ and C. Cyclic voltammetry (CV) was conducted in the voltage range of 0.0–3.0 V with a scan rate of 0.1 mV s⁻¹ using a CHI660D electrochemical workstation. Electrochemical impedance spectroscopy (EIS) was measured on a Zahner Elektrik electrochemical workstation in the frequency range of 0.01–100 kHz, which applied a DC potential equal to the open circuit voltage of the cell and an AC oscillation of 5 mV. The impedance data were analyzed by Z-view 2.0 software.

Results and discussion

Figure 1 shows the XRD patterns of Fe₃O₄ particles and Fe₃O₄/C nanoparticles. All peaks of the two samples are coincident with the standard for face-centered Fe₃O₄ (JCPDS No. 65-3107). No peak for impurities is detectable in the patterns. The existence of C in Fe₃O₄/C nanoparticles was confirmed by Raman spectroscopy (Fig. 2). It is clearly seen that the as-synthesized Fe₃O₄/C nanoparticles show a typical two-band Raman spectrum with D and G bands. The D band at ~1,337 cm⁻¹ is related to the vibrations of C atoms with dangling bonds in plane terminations of disordered graphite, confirming the amorphous C in the as-prepared material, while the G band at ~1,584 cm⁻¹ consists with the E_{2g} mode of graphite, namely, the stretching modes of C=C bonds of graphite (Dong et al. 2013). The result shows that there is amorphous C in the as-synthesized Fe₃O₄/C nanocomposites. Thermogravimetric analysis (TGA) was adopted to further confirm the C content in Fe₃O₄/C nanocomposites. Figure 3 is the TGA results of Fe₃O₄ particles and Fe₃O₄/C nanocomposites. As shown in Fig. 3, the mass loss of Fe₃O₄ particles and Fe₃O₄/C nanocomposites is little below 300 °C,

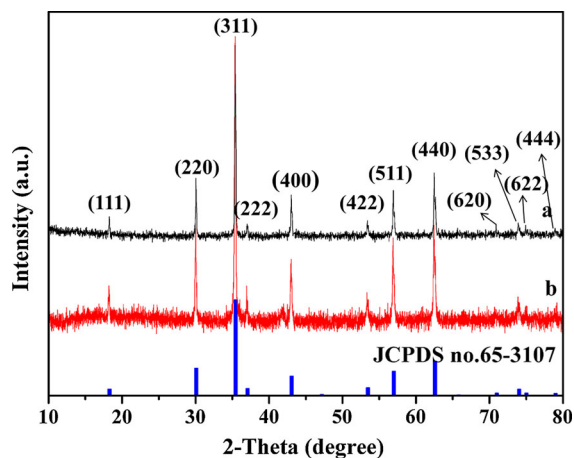


Fig. 1 XRD patterns of a Fe₃O₄ particles and b Fe₃O₄/C nanoparticles

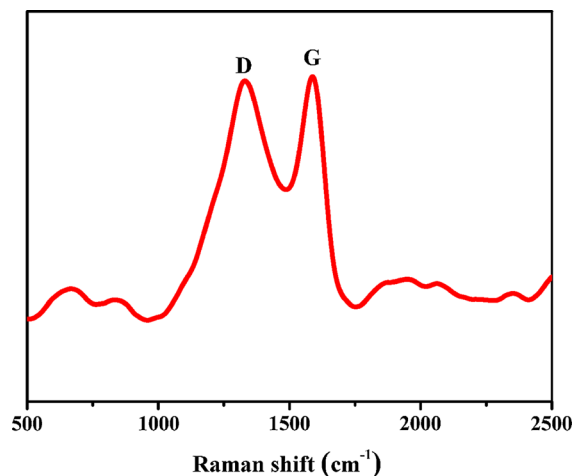


Fig. 2 Raman spectrum of Fe₃O₄/C nanocomposites

indicating the two samples are stable under air atmosphere. The mass of Fe₃O₄ particles and Fe₃O₄/C nanocomposites shows a small increase approximately at 300 °C due to the oxidation of partial Fe₃O₄ to Fe₂O₃ (Liu et al. 2012). After 300 °C, the mass of Fe₃O₄ particles is stable, while the mass of Fe₃O₄/C nanocomposites decreases from 300 to 500 °C and remains stable after 500 °C, which corresponds to C decomposition. Since Fe₃O₄/C nanocomposites were dried at 110 °C in a vacuum oven for 12 h before TG analysis, the release of water was negligible (Hu et al. 2014). Thus, the carbon content was considered as the total weight loss, which was calculated to be 8.9 wt%.

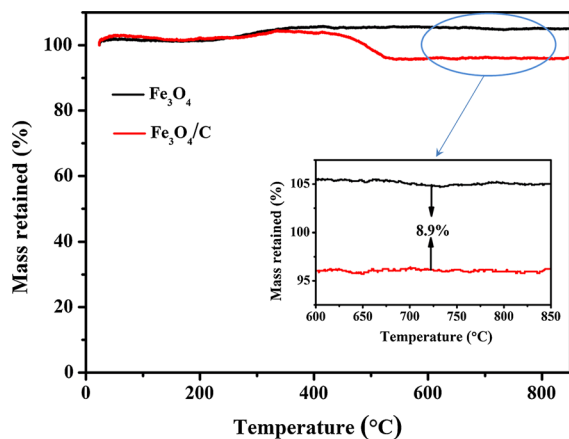
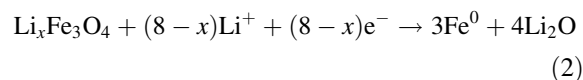
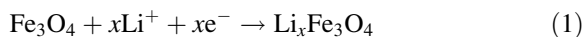


Fig. 3 TGA results of Fe_3O_4 particles and $\text{Fe}_3\text{O}_4/\text{C}$ nanocomposites. (Color figure online)

Figure 4 reveals the TEM images of Fe_3O_4 particles and $\text{Fe}_3\text{O}_4/\text{C}$ nanocomposites. It can be seen from Fig. 4a that Fe_3O_4 particles are aggregated. While in Fig. 4b the Fe_3O_4 nanoparticles and C nanoparticles can be clearly differentiated. C nanoparticles disperse among Fe_3O_4 particles forming a C layer, which prevents the Fe_3O_4 particles from contacting each other. The special structure of C nanoparticles can relieve the volume variation of Fe_3O_4 during charge/discharge process available (Huang et al. 2011). Furthermore, the existence of C nanoparticles limits the growth of Fe_3O_4 particles in the preparing procedure, which will prompt formation of $\text{Fe}_3\text{O}_4/\text{C}$ nanocomposites. The nanostructure of $\text{Fe}_3\text{O}_4/\text{C}$ is beneficial to shorten Li^+ diffusion path (Liu et al. 2012). Moreover, the C nanoparticles will improve

electrical conductivity (Zhang et al. 2008), suggesting that $\text{Fe}_3\text{O}_4/\text{C}$ nanocomposites possess better electrochemical performance.

Figure 5 shows the first five CV curves of Fe_3O_4 particles and $\text{Fe}_3\text{O}_4/\text{C}$ nanocomposites at room temperature in the voltage range of 0.0–3.0 V at a scanning rate of 0.1 mV s^{-1} . In the first cycle, both samples have a wide anodic peak located around 1.7–2.1 V, which corresponds to the reversible oxidation of Fe^0 to Fe^{2+} , and part to Fe^{3+} . Furthermore, two samples have a large cathodic polarization process (i.e., there is a voltage hysteresis during charge/discharge process) in the first cycle (about 0.58 V), which can be ascribed to electrolyte decomposition as well as SEI formation on the surface of the samples and Li^+ intercalation reaction as follows:



(He et al. 2013; Zhou et al. 2014).

The large polarization could be due to the poor conversion reaction kinetics (lithium diffusion kinetics is limited during the intercalation process, for example) (Mitra et al. 2006). The phenomenon of polarization has been widely observed in a number of other $\text{Fe}_3\text{O}_4/\text{C}$ composites (Zhang et al. 2008). Unfortunately, the application performance of LIBs is restricted by the large polarization. Therefore, it is very important to reduce the polarization of $\text{Fe}_3\text{O}_4/\text{C}$ nanocomposites in the future work by improving the conversion reaction kinetics, such as reducing the

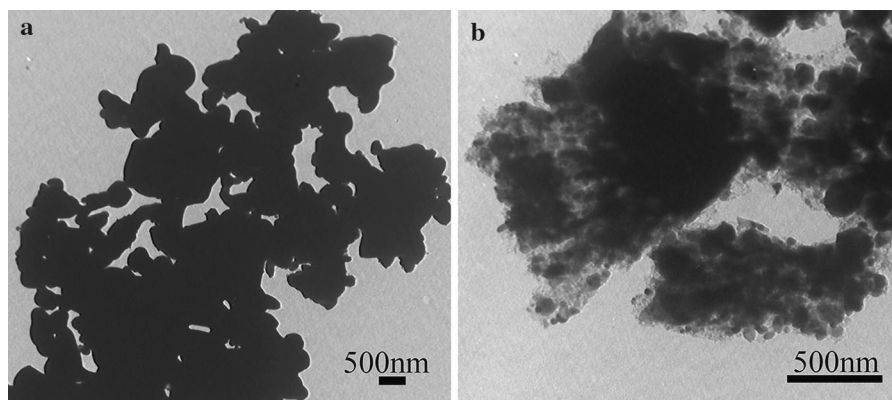


Fig. 4 TEM pattern of **a** Fe_3O_4 particles and **b** $\text{Fe}_3\text{O}_4/\text{C}$ nanocomposites

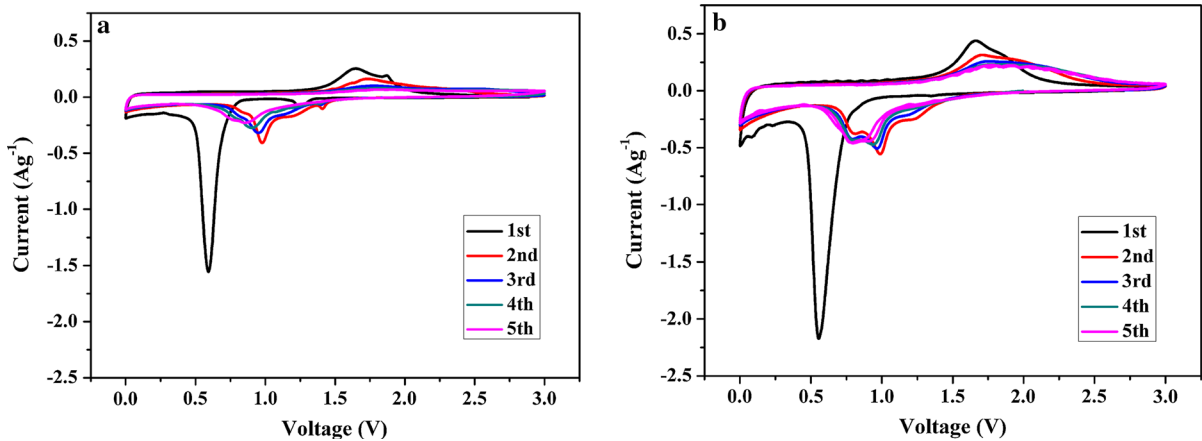


Fig. 5 Cyclic voltammograms of **a** Fe_3O_4 particles and **b** the $\text{Fe}_3\text{O}_4/\text{C}$ nanocomposites for the first 5 cycles. (Color figure online)

particle size of $\text{Fe}_3\text{O}_4/\text{C}$ nanocomposites (Lian et al. 2011). In the subsequent cycles, there is a substantial difference from the first cycle, which can be attributed to the decomposition of electrolyte to form a SEI layer. The peak current and integrated peak area of Fe_3O_4 are much lower than these of $\text{Fe}_3\text{O}_4/\text{C}$, indicating that $\text{Fe}_3\text{O}_4/\text{C}$ has higher capacity and reactivity than Fe_3O_4 . Besides the first cycle, the curves of $\text{Fe}_3\text{O}_4/\text{C}$ overlapped better than that of Fe_3O_4 , indicating that $\text{Fe}_3\text{O}_4/\text{C}$ has more stable structure and more excellent reversibility (Duan et al. 2012).

Figure 6 shows the initial charge/discharge curves of $\text{Fe}_3\text{O}_4/\text{C}$ nanocomposites and Fe_3O_4 particles at a current density of 1 C. As shown in Fig. 6, in the beginning, the voltage of both samples drops to 0.75 V quickly, which can be attributed to the reaction of $\text{Fe}_3\text{O}_4 + x\text{Li}^+ + xe^- \leftrightarrow \text{Li}_x\text{Fe}_3\text{O}_4$ (Wang et al. 2008), and then obvious potential plateau of both samples at about 0.75 V versus Li^+/Li , corresponding to the conversion reaction $\text{Li}_x\text{Fe}_3\text{O}_4 + (8-x)\text{Li}^+ \rightarrow 3\text{Fe}^0 + 4\text{Li}_2\text{O}$ (Wang et al. 2010). The sloping curve down to the cut-off voltage of 0.0 V can be ascribed to the reaction between Fe and the electrolyte that forms a gel-like solid electrolyte interphase (SEI) film (Laruelle et al. 2002). The $\text{Fe}_3\text{O}_4/\text{C}$ nanocomposites show a high discharge capacity of 1,480.4 mAh g^{-1} and a charge capacity of 903.5 mAh g^{-1} with a Coulombic efficiency of 61 % at the 1st cycle. While the Fe_3O_4 particles shows a discharge capacity of 1,255 mAh g^{-1} and a charge capacity of 857.7 mAh g^{-1} , the Coulombic efficiency of Fe_3O_4 particles is 68 % at the 1st cycle. The poor Coulombic efficiency for the first cycle of both

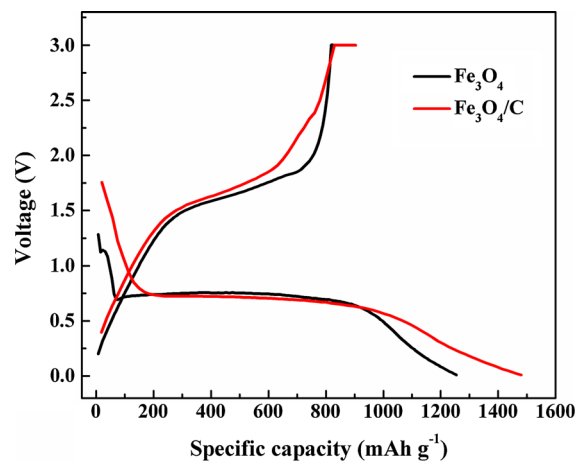


Fig. 6 The initial charge/discharge curves of Fe_3O_4 particles and $\text{Fe}_3\text{O}_4/\text{C}$ nanocomposites at 1 C. (Color figure online)

samples is ubiquitous for electrochemical reactions with lithium through a conversion reaction. (Cabana et al. 2010). Compared to Fe_3O_4 particles, $\text{Fe}_3\text{O}_4/\text{C}$ nanocomposites have lower first Coulomb efficiency, the $\text{Fe}_3\text{O}_4/\text{C}$ nanocomposites with lower first Coulomb efficiency possibly originates from the existence of amorphous C, which has a high surface area (Zhao et al. 2012b). The reason needs further investigation. However, lower first Coulombic efficiency of the $\text{Fe}_3\text{O}_4/\text{C}$ nanocomposites needs further improvement. The cycling performance of Fe_3O_4 particles and $\text{Fe}_3\text{O}_4/\text{C}$ nanocomposites was evaluated between 0.0 and 3.0 V at 1 C for 110 cycles. As shown in Fig. 7, the first discharge capacity of Fe_3O_4 particles is as high as 1,255 mAh g^{-1} .

However, the discharge capacity quickly fades and only 317.4 mAh g⁻¹ remains at the 110th cycle, indicating Fe₃O₄ particles have a poor cycling performance (Chen et al. 2011a). In contrast, the first discharge capacity of Fe₃O₄/C nanocomposites is as high as 1,480.4 mAh g⁻¹, and stabilizes at 902.4 mAh g⁻¹ after 110 cycles. Obviously, the cycling performance and specific capacity of Fe₃O₄/C nanocomposites are much better than those of Fe₃O₄ particles and many other similar materials reported (Lang and Xu 2013; Li et al. 2012b; Zhao et al. 2012a). Fe₃O₄/Fe/C, which prepared by Zhao et al., exhibited about 600 mAh g⁻¹ capacity at 50 mA g⁻¹ after 40 cycles; Lang et al. prepared porous Fe₃O₄/C microbelts, which exhibited a 710 mAh g⁻¹ capacity at 0.2 C after 50 cycles; Fe₃O₄@C core-shell rings prepared by Li et al. showed 801 mAh g⁻¹ at 0.2 C after 100 cycles. Compared to the materials, the cycling performance of Fe₃O₄/C nanocomposites in this paper is even better, indicating that the one-pot PEG-assisted co-precipitation method could be an effective and simple way to synthesize Fe₃O₄/C nanocomposites with excellent electrochemical performance. Herein, both of the initial discharge capacities of Fe₃O₄ particles (1,255 mAh g⁻¹) and Fe₃O₄/C nanocomposites (1,480.4 mAh g⁻¹) exceed the theoretical capacity of Fe₃O₄ (924 mAh g⁻¹). The extra capacities of the two samples beyond the theoretical values are probably due to the decomposition of non-aqueous electrolyte during the discharge process (Huang et al. 2011). It has been reported that, during the charge/discharge process, the Fe₃O₄-based anode surface would be covered by SEI film, which formed due to the reductive decomposition of the organic electrolyte. And the capacity of Fe₃O₄ mainly comes from the reversible conversion reaction between Li⁺ and Fe₃O₄. During lithiation, a Li₂O matrix was formed, and Fe nanocrystals dispersed in this matrix [Li₂O and Fe formed from above Eqs. (1) and (2)]. The Fe nanocrystals can catalyze decomposition of the SEI. For Fe₃O₄/C nanocomposites obtained in this work, the C layer which dispersed among Fe₃O₄ particles can prevent Fe nanocrystals from catalyzing decomposition of the outer SEI. Thus, a relative stable SEI film would form on the materials surface without the rupturing and reformation, which reduced depletion of the electrolyte. Furthermore, the C layer can accommodate the volume expansion/contraction of Fe₃O₄ particles upon lithiation/delithiation without breaking down the structure of Fe₃O₄/C nanocomposites. So Fe₃O₄/C nanocomposites

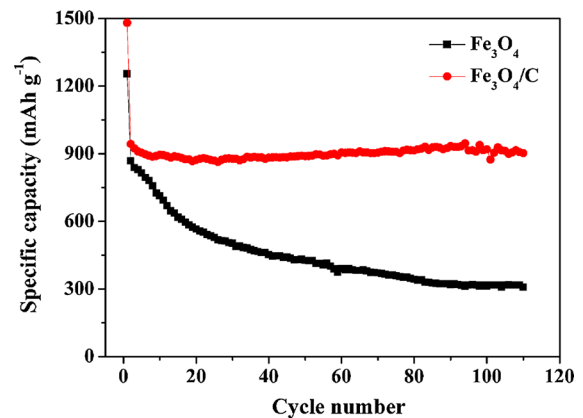


Fig. 7 Cycling performance of Fe₃O₄ particles and Fe₃O₄/C nanocomposites at 1 C. (Color figure online)

possess excellent cycling performance and high capacity (He et al. 2013). However, both Fe₃O₄ particles and Fe₃O₄/C nanocomposites have a large polarization in the first cycle may be caused by conversion of Fe₃O₄ to Fe and the consumption of the electrolyte to form SEI, this characteristic is agreed well with the CV results.

Besides the high capacity and stable cycling performance, a good rate performance is also an important criterion for high performance of LIBs. Figure 8 is cycling performance of Fe₃O₄ particles and Fe₃O₄/C nanocomposites at various current densities (100–1,500 mA g⁻¹) at room temperature. As show in Fig. 8, Fe₃O₄/C nanocomposites are capable of delivering discharge capacity of 1,053.4, 981.1, 894.4, 866.9, 808.9, and 698.3 mAh g⁻¹ at the current density of 100, 200, 500, 700, 1,000, and 1,500 mA g⁻¹, respectively. After charge/discharge cycling at high current density, the current density is reduced stepwise to 100 mA g⁻¹, with a specific capacity as high as 1,086.7 mAh g⁻¹ recovered, indicating that Fe₃O₄/C nanocomposites have good kinetic properties (Lian et al. 2010). Remarkably, the discharge capacities of Fe₃O₄/C nanocomposites at current densities of 100 and 200 mA g⁻¹ are higher than the theoretical capacity of Fe₃O₄. The extra capacity may be due to the synergistic effect between Fe₃O₄ nanoparticles and C layer in the nanocomposites under small current densities (Paek et al. 2009), and the real reason needs further investigation. However, as the current density increases from 100 to 200, 500, 700, 1,000, and 1,500 mA g⁻¹, the reversible capacity of Fe₃O₄ decreases from 722.5 to 496.2, 411.2, 317.3, 250.7, and 173.2 mAh g⁻¹, respectively. Fe₃O₄/C nanocomposites display superior rate

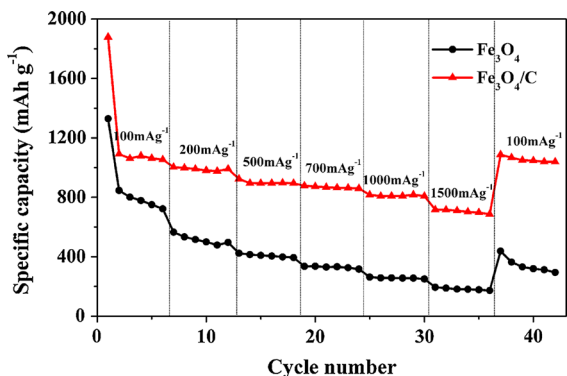


Fig. 8 Cycling performance of Fe₃O₄ particles and Fe₃O₄/C nanocomposites at various current densities (100–1,500 mA g⁻¹). (Color figure online)

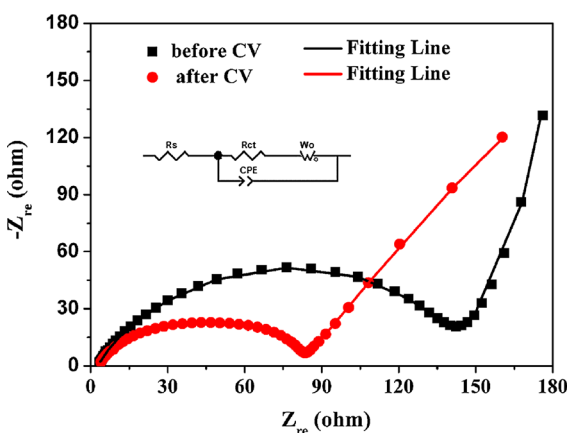


Fig. 9 Electrochemical impedance spectra of Fe₃O₄/C nanocomposites before and after cyclic voltammograms, with the inset showing equivalent circuit model used for fitting. (Color figure online)

capability and reversibility compared with previously reported results. Fe₃O₄/Fe/C (Zhao et al. 2012a) was prepared by sol-gel method with ultrasonication and vacuum drying, it exhibited about 500 mAh g⁻¹ capacity at the current density of 500 mA g⁻¹; porous Fe₃O₄/C microbelts (Lang and Xu 2013) were prepared by electrostatic spinning, which including complicated steps such as selection of viscosity and ultrasonic. And the prepared Fe₃O₄/C microbelts exhibited a capacity of 300 mAh g⁻¹ at the current rate of 1 C. By contrast, herein Fe₃O₄/C nanocomposites were prepared by a simple one-pot PEG-assisted co-precipitation method, and the as-prepared Fe₃O₄/C nanocomposites have ultra-high rate capabilities. The much improved electrochemical performance of Fe₃O₄/C nanocomposites could be explained as follows: Firstly, Raman

spectroscopy data show that there are amorphous C nanoparticles in Fe₃O₄/C nanocomposites. The existence of amorphous C in the composite materials not only buffers the volume expansion/contraction of Fe₃O₄ during charge/discharge process, but also restrains the growth of Fe₃O₄ particles to easily form Fe₃O₄/C nanocomposites (Huang et al. 2011). Nanocomposites with small size will shorten Li⁺ diffusion path and make the permeation of electrolyte easier to surface of electrode, which will accelerate electrochemistry reaction (Duan et al. 2012). Secondly, the amorphous C can form a conducting network to enhance the electrical conductivity of Fe₃O₄/C nanocomposites, which will improve the electrochemical performance of the nanocomposites (Zhang et al. 2008). Thirdly, The TEM shows that C surrounding the Fe₃O₄ particles; the C layer which surrounded Fe₃O₄ nanoparticles build a special nanostructure, which can prevent Fe nanocrystals from catalyzing decomposition the outer SEI. Thus, a relatively stable SEI film would form on the material surface without rupturing and reformation. The stable SEI guaranteed excellent cycling performance and high capacity of Fe₃O₄/C nanocomposites (He et al. 2013).

In order to understand the impedance changes of Fe₃O₄/C nanocomposites, electrochemical impedance spectroscopy (EIS) measurements of the composites conducted on the fresh battery and the battery after CV tested. The impedance data were analyzed with Z-view 2.0 software by fitting to an equivalent electrical circuit, which show in Fig. 9. *R_s* is the bulk solution resistance; *R_{ct}* is charge-transfer resistance; *W_o* is the Warburg impedance describing the diffusion of Li⁺ in Fe₃O₄/C; CPE reflects the interfacial capacitance (Li et al. 2012a). Each spectrum is consists of a semicircle in the high-frequency region and a straight line in the low-frequency region. The depressed semicircle in high-frequency region is attributed to the charge-transfer resistance (*R_{ct}*) of the electrochemical reaction and the straight line is related to the diffusion-controlled Warburg impedance. From the fitted results, the charge-transfer resistance of the fresh battery is (~148.1 Ω) higher than that of the battery after CV tested (~82.6 Ω), due to the wetting of Fe₃O₄/C by electrolyte. After CV tested, the battery aging as well as continuous electrochemical interaction, the electrode of fully wetting by electrolyte provided continuous transportation paths, which enhanced Li⁺ diffusion and decreased the impedance as well as improved the

electrochemical performance of Fe₃O₄/C (Tummala et al. 2012).

Conclusion

Fe₃O₄/C nanocomposites were prepared by one-pot PEG-assisted co-precipitation method with simple steps. The XRD and TEM results show that Fe₃O₄/C nanocomposites are well crystallized and a matrix is formed by conductive C surrounding Fe₃O₄ particles. The as-synthesized Fe₃O₄/C nanocomposites exhibit excellent electrochemical performance with a stable specific discharge capacity of 902.4 mAh g⁻¹ after 110 cycles at 1 C and ultra-high rate capabilities. Compared with other nanosized Fe-based materials, the electrochemical performance of Fe₃O₄/C nanocomposites is improved obviously. Taking the excellent electrochemical performance and facile synthesis method into consideration, Fe₃O₄/C nanocomposites prepared by one-pot PEG-assisted co-precipitation method could be a competitive candidate anodic material for high-performance LIBs in the future.

Acknowledgments This work was supported by the Natural Science Foundation of Xinjiang Province (2013211A004).

References

- Bruce PG, Scrosati B, Tarascon JM (2008) Nanomaterials for rechargeable lithium batteries *Angew Chem. Int Ed* 47:2930–2946. doi:10.1002/anie.200702505
- Cabana J, Monconduit L, Larcher D, Palacín MR (2010) Beyond intercalation-based Li-ion batteries: the state of the art and challenges of electrode materials reacting through conversion reactions. *Adv Mater* 22:E170–E192. doi:10.1002/adma.201090116
- Chen JS, Zhang YM, Lou XW (2011a) One-pot synthesis of uniform Fe₃O₄ nanospheres with carbon matrix support for improved lithium storage capabilities. *ACS Appl Mater Interfaces* 3:3276–3279
- Chen YJ, Xiao G, Wang TS, Ouyang QY, Qi LH, Ma Y, Gao P, Zhu CL, Cao MS, Jin HB (2011b) Porous Fe₃O₄/carbon core/shell nanorods: synthesis and electromagnetic properties. *J Phys Chem C* 115:13603–13608. doi:10.1021/jp202473y
- Chen Y, Song B, Tang X, Lu L, Xue J (2012a) One-step synthesis of hollow porous Fe₃O₄ beads-reduced graphene oxide composites with superior battery performance. *J Mater Chem* 22:17656–17662. doi:10.1039/c2jm32057f
- Chen Y, Xia H, Lu L, Xue J (2012b) Synthesis of porous hollow Fe₃O₄ beads and their applications in lithium ion batteries. *J Mater Chem* 22:5006. doi:10.1039/c2jm15440d
- Dong Y, Hu M, Ma R, Cheng H, Yang S, Li YY, Zapien JA (2013) Evaporation-induced synthesis of carbon-supported Fe₃O₄ nanocomposites as anode material for lithium-ion batteries. *CrystEngComm* 15:1324. doi:10.1039/c2ce26459e
- Duan L, Huang Y, Jia D, Wang X, Guo Z (2012) Fe₃O₄ fuzzy spheroids as anode materials for lithium-ion batteries. *Mater Lett* 71:151–153. doi:10.1016/j.matlet.2011.12.051
- Gao G et al (2011) One-step synthesis of Fe₃O₄@C nanotubes for the immobilization of adriamycin. *J Mater Chem* 21:12224. doi:10.1039/c1jm12535d
- Gong C, Xue Z, Wang X, Zhou XP, Xie XL, Mai YW (2014) Poly(ethylene glycol) grafted multi-walled carbon nanotubes/LiFePO₄ composite cathodes for lithium ion batteries. *J Power Sources* 246:260–268. doi:10.1016/j.jpowsour.2013.07.091
- He C, Wu S, Zhao N, Shi C, Liu E, Li J (2013) Carbon-encapsulated Fe₃O₄ nanoparticles as a high-rate lithium ion battery anode material. *ACS Nano* 4:4459–4469
- Hu M, Jiang Y, Yan M (2014) Scalable synthesis of Fe₃O₄/C composites with enhanced electrochemical performance as anode materials for lithium-ion batteries. *J Alloys Compd* 582:563–568. doi:10.1016/j.jallcom.2013.08.098
- Huang Y, Dong Z, Jia D, Guo Z, Cho WI (2011) Preparation and characterization of core-shell structure Fe₃O₄/C nanoparticles with unique stability and high electrochemical performance for lithium-ion battery anode material. *Electrochim Acta* 56:9233–9239. doi:10.1016/j.electacta.2011.07.141
- Lang L, Xu Z (2013) In situ synthesis of porous Fe₃O₄/C microbelts and their enhanced electrochemical performance for lithium-ion batteries. *ACS Appl Mater Interfaces* 5:1698–1703. doi:10.1021/am302753p
- Laruelle S, Gugon S, Poizot P, Dollé M, Dupont L, Tarascon JM (2002) On the origin of the extra electrochemical capacity displayed by MO/Li cells at low potential. *J Electrochem Soc* 149:A627–A634. doi:10.1149/1.1467947
- Li L, Wang T, Zhang L, Su Z, Wang C, Wang R (2012a) Selected-control synthesis of monodisperse Fe₃O₄@C core-shell spheres, chains, and rings as high-performance anode materials for lithium-ion batteries. *Chem Eur J* 18:11417–11422. doi:10.1002/chem.201200791
- Li R, Ren X, Zhang F, Du C, Liu J (2012b) Synthesis of Fe₃O₄@SnO₂ core-shell nanorod film and its application as a thin-film supercapacitor electrode. *Chem Commun* 48:5010–5012. doi:10.1039/c2cc31786a
- Lian P, Zhu X, Liang S, Li Z, Yang W, Wang H (2010) Large reversible capacity of high quality graphene sheets as an anode material for lithium-ion batteries. *Electrochim Acta* 55:3909–3914. doi:10.1016/j.electacta.2010.02.025
- Lian P, Zhu X, Liang S, Li Z, Yang W, Wang H (2011) High reversible capacity of SnO₂/graphene nanocomposite as an anode material for lithium-ion batteries. *Electrochim Acta* 56:4532–4539. doi:10.1016/j.electacta.2011.01.126
- Liu J, Zhou Y, Liu F, Liu C, Wang J, Pan Y, Xue D (2012) One-pot synthesis of mesoporous interconnected carbon-encapsulated Fe₃O₄ nanospheres as superior anodes for Li-ion batteries. *RSC Adv* 2:2262–2265. doi:10.1039/c2ra01241c
- Mitra S, Poizot P, Finke A, Tarascon JM (2006) Growth and electrochemical characterization versus lithium of Fe₃O₄ electrodes made by electrodeposition. *Adv Funct Mater* 16:2281–2287. doi:10.1002/adfm.200500753

- Paek SM, Yoo EJ, Honma I (2009) Enhanced cyclic performance and lithium storage capacity of SnO₂/graphene nanoporous electrodes with three-dimensionally delaminated flexible structure. *Nano Lett* 9:72–75
- Tummala R, Guduru RK, Mohanty PS (2012) Binder free, porous and nanostructured Co₃O₄ anode for Li-ion batteries from solution precursor plasma deposition. *J Power Sources* 199:270–277. doi:[10.1016/j.jpowsour.2011.10.048](https://doi.org/10.1016/j.jpowsour.2011.10.048)
- Wang L, Yu Y, Chen PC, Zhang DW, Chen CH (2008) Electrospinning synthesis of C/Fe₃O₄ composite nanofibers and their application for high performance lithium-ion batteries. *J Power Sources* 183:717–723. doi:[10.1016/j.jpowsour.2008.05.079](https://doi.org/10.1016/j.jpowsour.2008.05.079)
- Wang SQ, Zhang JY, Chen CH (2010) Fe₃O₄ submicron spheroids as anode materials for lithium-ion batteries with stable and high electrochemical performance. *J Power Sources* 195:5379–5381. doi:[10.1016/j.jpowsour.2010.03.035](https://doi.org/10.1016/j.jpowsour.2010.03.035)
- Wu P, Du N, Zhang H, Yu J, Yang D (2011) Carbon nanocapsules as nanoreactors for controllable synthesis of encapsulated iron and iron oxides: magnetic properties and reversible lithium storage. *J Phys Chem C* 115:3612–3620. doi:[10.1021/jp1113653](https://doi.org/10.1021/jp1113653)
- Zhang WM, Wu XL, Hu JS, Guo YG, Wan LJ (2008) Carbon coated Fe₃O₄ nanospindles as a superior anode material for lithium-ion batteries. *Adv Funct Mater* 18:3941–3946. doi:[10.1002/adfm.200801386](https://doi.org/10.1002/adfm.200801386)
- Zhao X, Xia D, Zheng K (2012a) Fe₃O₄/Fe/carbon composite and its application as anode material for lithium-ion batteries. *ACS Appl Mater Interfaces* 4:1350–1356. doi:[10.1021/am201617j](https://doi.org/10.1021/am201617j)
- Zhao X, Xia D, Zheng K (2012b) An Fe₃O₄-FeO-Fe@C composite and its application as anode for lithium-ion battery. *J Alloys Compd* 513:460–465. doi:[10.1016/j.jallcom.2011.10.081](https://doi.org/10.1016/j.jallcom.2011.10.081)
- Zhong Y, Wang X, Jiang K, Zheng JY, Guo Y, Ma Y, Yao J (2011) A facile synthesis and lithium storage properties of Co₃O₄/C hybrid core-shell and hollow spheres. *J Mater Chem* 21:17998–18002. doi:[10.1039/c1jm12765a](https://doi.org/10.1039/c1jm12765a)
- Zhou Q, Zhao Z, Wang Z, Dong Y, Wang X, Gogotsi Y, Qiu J (2014) Low temperature plasma synthesis of mesoporous Fe₃O₄ nanorods grafted on reduced graphene oxide for high performance lithium storage. *Nanoscale* 6:2286–2291. doi:[10.1039/c3nr05423c](https://doi.org/10.1039/c3nr05423c)